RSC Advances

PAPER

View Article Online
View Journal | View Issue

Cite this: *RSC Adv.*, 2024, **14**, 38605

Magnetically retrievable carbon-wrapped CNT/Ni nanospheres as efficient catalysts for nitroaromatic reduction

Sumaya Nur Mithila, [a] Akter Hossain Reaz, [ab] Fatema Zerin Farhana, [ac] Muhammad J. A. Shiddiky *[c] and Shakhawat H. Firoz *[a]

We present a facile strategy for synthesizing magnetically retrievable carbon-wrapped CNT/Ni nanospheres (C-wrapped CNT/Ni) that enhance the catalytic performance of metals for environmental pollutant reduction. Structural and compositional analyses using X-ray diffraction (XRD), Raman spectroscopy, energy-dispersive X-ray spectroscopy (EDS), and field emission scanning electron microscopy (FESEM) confirmed the phase purity, morphology, and structure of the C-wrapped CNT/Ni. XRD, Raman, and EDS data validate the formation of the nanospheres, while FESEM images reveal uniform Ni nanospheres wrapped with a carbon layer through interconnected, evenly dispersed CNTs. Initially, Ni nanoparticles were anchored onto multiwalled carbon nanotubes to form magnetic CNT/Ni nanospheres, which were then coated with a carbon layer to prevent aggregation, improve Ni particle stability, and introduce additional surface functionalities. The catalytic efficacy of C-wrapped CNT/Ni was assessed through the reduction of 4-nitrophenol (4-NP) to 4-aminophenol (4-AP). The reaction rate constant (k_{app} = 0.6167 min^{-1}) with C-wrapped CNT/Ni is approximately six times higher than that with bare Ni nanospheres (k_{app} = 0.1056 min^{-1}). This enhanced catalytic activity is attributed to the synergistic effect between the spherical Ni core and the wrapped carbon layer, mediated by the interconnected CNT, which promotes efficient hydride formation. Additionally, C-wrapped CNT/Ni demonstrates exceptional reusability in the 4-NP reduction process. The integration of these features within a single framework suggests its significant potential for diverse engineering and environmental applications.

Received 2nd November 2024
Accepted 2nd December 2024

DOI: 10.1039/d4ra07815b

rsc.li/rsc-advances

1. Introduction

The rapid growth of industrial and agricultural activities has led to the unregulated release of untreated wastewater containing toxic contaminants such as nitroaromatics and dyes, presenting significant environmental challenges.[1] Nitroaromatic compounds, commonly found in industrial effluents from explosives, pesticides, pharmaceuticals, and other sources, include hazardous pollutants like 4-nitrophenol (4-NP).[2] 4-NP, a phenolic compound with a benzene ring and a nitro ($-NO_2$) group, poses severe health risks including blood disorders, nervous system damage, and organ failure due to bioaccumulation.[3] Its high solubility in water increases its bioavailability and potential harm to ecosystems. To protect the environment and human health, the US Environmental Protection Agency has set a stringent limit of 10 ng L^{-1} for 4-NP in aquatic environments.[4]

Various methods for removing 4-NP have been explored, including adsorption,[5] biodegradation,[6] electrocoagulation,[7] photocatalysis,[8] and electrochemical degradation.[9] However, these methods often suffer from limitations such as low efficacy, long operation times, and high costs. Catalytic conversion of 4-NP to 4-aminophenol (4-AP) using $NaBH_4$ has emerged as a promising alternative due to its efficiency, cleanliness, and cost-effectiveness.[10] Given the importance of 4-AP as an intermediate for antipyretic and analgesic compounds like phenacetin and acetanilide,[11] the development of effective catalysts is crucial for addressing health and environmental challenges associated with nitroaromatics.

Efficient catalysts typically require excellent adsorption properties and remarkable electron transport abilities.[12] While noble metal nanoparticles (Au, Pt, Pd, Ag) exhibit high catalytic activity, their high cost and limited availability restrict their practical use.[13–15] As a result, there is growing interest in non-noble metal-based catalysts, particularly nanostructured transition metal nanoparticles (TMNPs) such as Cu, Ni, and Co.[16–20] Nickel nanoparticles (Ni NPs) are promising due to their structural and magnetic properties, high selectivity, efficient electron transport capabilities, and excellent recyclability.[13,21] Additionally, magnetism plays a vital role in material recovery

[a]*Department of Chemistry, Bangladesh University of Engineering and Technology, Dhaka 1000, Bangladesh. E-mail: shfiroz@chem.buet.ac.bd*

[b]*Department of Chemistry, Michigan State University, East Lansing, MI 48824, USA*

[c]*Rural Health Research Institute, Charles Sturt University, Orange, NSW 2800, Australia. E-mail: mshiddiky@csu.edu.au*

for catalytic processes by enabling efficient separation and reuse of magnetic catalysts. Magnetic nanoparticles, for instance, can be easily retrieved from reaction mixtures using external magnetic fields, reducing material loss and simplifying recovery processes. This approach enhances sustainability, minimizes waste, and lowers costs, making catalytic systems more environmentally friendly and economically viable. The use of magnetically recoverable catalysts has shown significant potential in green chemistry applications.[22]

However, their catalytic activity often falls short compared to noble metal catalysts. Strategies to improve Ni NPs' performance include immobilization to reduce aggregation and the use of controlled nanoarchitectures to enhance the surface area-to-volume ratio, which could provide more active catalytic sites. Despite these efforts, small-sized Ni nanospheres remain highly aggregable and unstable due to their high surface energy and reactivity, limiting their catalytic efficiency.[17–20]

Carbon-based materials offer a viable solution as supports and carriers for nanomaterials due to their high surface area, conductivity, chemical inertness, thermal stability, and mechanical strength.[18,20,23] Carbon-coated TMNPs have garnered attention because the carbon shell enhances stability and prevents oxidation and agglomeration of metal nanoparticles. Additionally, carbon encapsulation can improve the electronic density of states of the outer shell carbon atoms, facilitating charge transport and enhancing catalytic activity. Various carbon materials, such as carbon black, mesoporous carbon, graphene, and carbon fabric, have been used to support or coat TMNPs, improving their catalytic activities.[24–26] However, many of these supports do not effectively contribute to catalytic processes, particularly in hydride formation for 4-NP reduction. Furthermore, existing methods for synthesizing carbon-coated TMNPs, especially Ni nanospheres, often involve complex procedures and are not suitable for large-scale applications.

To address these challenges, carbon nanotubes (CNTs) offer a promising alternative due to their exceptional properties, including high surface area, superior electron conductivity, chemical inertness, and mechanical strength.[27] CNTs' unique characteristics, such as their interior tunnelling properties and surface charge, can influence catalytic reactions by redistributing π electron density and enhancing electron transport.[28] Incorporation of CNTs and carbon shell into Ni nanospheres can improve the electronic density of states and enhance catalytic activity by facilitating hydride formation and improving product absorption and desorption.

Although CNT-based catalysts have been explored in hydrogenation reactions and the reduction of nitroaromatic compounds,[29–32] challenges such as complex synthesis and low catalytic efficiency have limited their large-scale application. Thus, C-wrapped CNT/Ni nanospheres presents a novel approach to enhance the distribution of electronic environments and regulate Ni nanospheres' aggregation. This method aims to create highly efficient heterogeneous catalysts for reducing 4-NP by improving electron transfer and hydride generation. To our knowledge, the fabrication of C-wrapped CNT/Ni nanospheres for 4-NP reduction has not been reported. In this study, we propose a novel and straightforward method for synthesizing magnetically retrievable C-wrapped CNT/Ni nanospheres and investigate their catalytic performance and mechanistic pathways for reducing nitroaromatics.

2. Experimental

2.1 Materials

Sodium hydroxide (NaOH), nickel chloride hexahydrate ($NiCl_2 \cdot 6H_2O$), hydrazine hydrate ($N_2H_4 \cdot H_2O$, 80%), tri-ethylene glycol (TEG), and carbon nanotubes (CNT) were procured from Sigma-Aldrich and were of analytical grade, used as received without further purification. Deionized water, essential for solution preparation, was obtained using a Barnstead nanopure water system (Thermo Scientific, USA). The hydrothermal process was conducted in a Teflon-lined stainless-steel autoclave (HYD-100, TEFIC Biotech, China), and a Muffle furnace (LT 5/12, Nabertherm, Germany) was utilized for heat treatment. Ultrasonication was performed in a digitally controlled ultrasonic bath (Powersonic 505, Hwashin, S. Korea) to ensure proper mixing and dispersion.

2.2 Preparation of Ni nanospheres

Ni nanospheres were synthesized *via* a reduction method using nickel chloride and hydrazine hydrate in the presence of sodium hydroxide. The reaction was conducted with a molar ratio of 0.135 : 0.45 : 0.36 ($NiCl_2 : N_2H_4 : NaOH$) to control the size of the nanospheres. Specifically, 0.135 mol of $NiCl_2 \cdot 6H_2O$ (32.13 g) was dissolved in 37.5 g of water and then added to 0.45 mol of 80% $N_2H_4 \cdot H_2O$ (28.22 g) in a 100 cm^3 round-bottom flask under vigorous stirring. This resulted in the formation of a pale violet precipitate. The flask walls were rinsed with 5–10 g of deionized (DI) water for approximately 60 seconds. As a complex formed between Ni^{2+} and N_2H_4, the solution temperature increased to 65 °C and then was allowed to cool to 50 °C while stirring continued. Subsequently, 28.8 g of a cold aqueous NaOH solution (50%) was added when the temperature reached 50 °C. The addition of NaOH caused the temperature to rise again to 54 °C due to the formation of Ni $(OH)_2$. The reaction mixture was stirred for one hour, gradually converting the Ni complex into Ni nanoparticles (NPs), resulting in the formation of a black precipitate of Ni nanospheres. The product was washed thoroughly with DI water and ethanol, and then dried at room temperature for 24 hours under constant ventilation.

2.3 Preparation of carbon-wrapped Ni nanospheres

Carbon-wrapped Ni nanospheres were prepared through the hydrothermal treatment of tri-ethylene glycol (TEG) with the pre-synthesized Ni nanospheres. In this process, 1 g of Ni nanospheres was dispersed in 30 mL of TEG by vigorous stirring. The resulting mixture was transferred to a 50 mL Teflon-lined autoclave and heated in a muffle furnace at 250 °C for 12 hours. After cooling to room temperature, the product was collected, washed multiple times with DI water, and dried for 24 hours under constant ventilation.

2.4 Fabrication of carbon-wrapped CNT/Ni nanospheres

Carbon-wrapped CNT/Ni nanospheres were synthesized by integrating pre-dispersed CNTs with the reduction of $NiCl_2 \cdot 6H_2O$ using $N_2H_4 \cdot H_2O$. Initially, 50 mg of CNT was dispersed in 10 mL of DI water through sonication and then combined with 32.13 g of $NiCl_2 \cdot 6H_2O$ (0.135 mol) in a 100 cm^3 round-bottom flask. The resulting greenish-black solution was stirred vigorously for 30 minutes. Subsequently, 28.12 g of 80% $N_2H_4 \cdot H_2O$ (0.451 mol) was added slowly to the mixture, leading to the formation of a pale violet-blackish precipitate as the temperature increased to 60 °C. The precipitate was rinsed from the flask walls with 5–10 g of DI water and allowed to cool to 50 °C. A cold aqueous solution of 50% NaOH (28.8 g) was then added, and the mixture was stirred at 54 °C for one hour, resulting in the formation of black CNT/Ni nanospheres. The product was washed thoroughly with DI water and ethanol before being dried in a vacuum oven at 40 °C for 16 hours. To obtain carbon-wrapped CNT/Ni nanospheres, 1.0 g of the pre-synthesized CNT/Ni nanosphere was dispersed in 30 mL of TEG and placed in a 50 mL Teflon-lined autoclave. The mixture underwent hydrothermal treatment at 250 °C for 12 hours. After cooling, the product was washed with DI water and ethanol and dried in a vacuum oven at 40 °C for 24 hours.

The synthesis process for the C-wrapped CNT/Ni nanosphere catalyst is illustrated in Fig. 1. Initially, nickel(II) chloride was reduced using hydrazine hydrate in the presence of sodium hydroxide, leading to the formation of Ni nanospheres. The addition of NaOH initiated a series of reactions starting with the complex formation between nickel(II) chloride and hydrazine. This complex subsequently decomposed, resulting in the formation of a $Ni(OH)_2$ gel, which was eventually reduced to metallic Ni nanospheres.[33]

During the formation of Ni nanospheres, dispersed CNTs interacted with the nanospheres due to surface charge interactions, promoting a strong attachment. A thin coating of triethylene glycol (TEG) was then applied to the pre-synthesized CNT/Ni nanospheres. This coating was converted into a carbon layer through low-temperature carbonization during hydrothermal treatment, ultimately producing C-wrapped CNT/Ni nanospheres.

2.5 Characterization

The phase purity and structural properties of the synthesized samples were analysed using X-ray powder diffraction (XRD) on a Rigaku Smart Lab X-ray diffractometer with Cu-Kα radiation ($\lambda = 1.5406$ Å) at a scanning rate of 2.0° min^{-1} over a 10–80 degree range. The morphology of the samples was examined using Field Emission Scanning Electron Microscopy (FESEM; JSM-7600F, Tokyo, Japan) at an accelerating voltage of 10 kV. Energy-dispersive X-ray spectroscopy (EDX) was also performed on the same instrument. UV-vis spectroscopy was conducted using a Shimadzu-1800 spectrophotometer (Hitachi, Japan), and Raman spectra were recorded using a Metrohm Raman, MIRA XTR spectrometer.

2.6 Catalytic reduction of 4-nitrophenol

The catalytic activity of the carbon-wrapped CNT/Ni nanospheres was evaluated using the reduction of 4-nitrophenol (4-NP) to 4-aminophenol (4-AP) with excess $NaBH_4$ as a model reaction. A reaction mixture was prepared by adding 300 μL of a 1 mM 4-NP solution and 1 mL of a 10 mM $NaBH_4$ solution to 5 mL of DI water into a 25 mL glass vial. The formation of the phenolate ion was observed by a color change from pale yellow to bright yellow and confirmed by UV-vis spectroscopy, with an absorbance peak at 400 nm.

For the catalytic experiment, 1 mL of a carbon-wrapped CNT/Ni nanosphere suspension (4 mg mL^{-1}) was added to the reaction mixture. The progress of the reaction was monitored using UV-vis spectroscopy with a time interval until the solution turned colourless, indicating complete reduction of 4-NP.

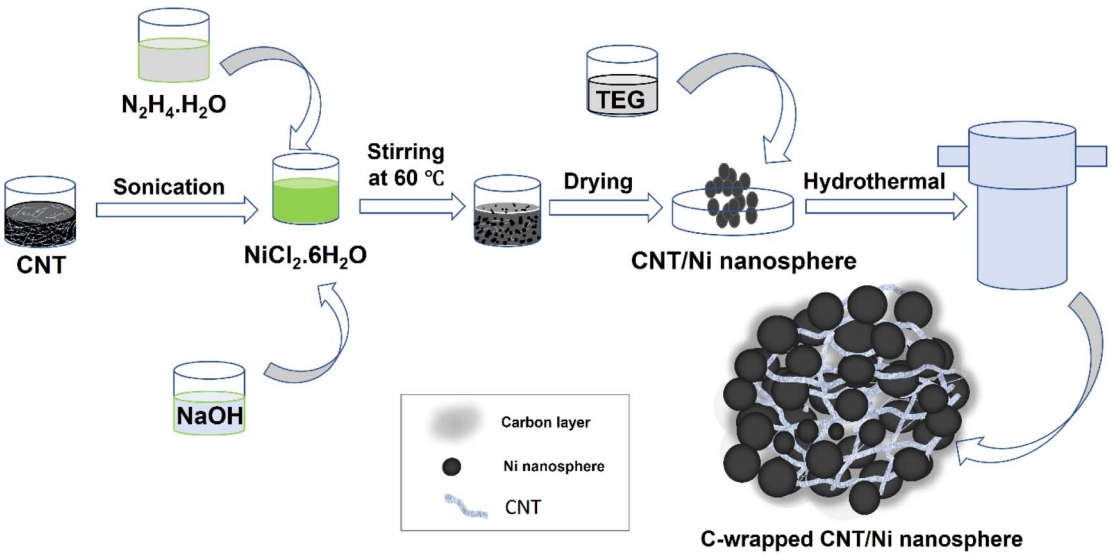

Fig. 1 Schematic illustration of the preparation process for carbon-wrapped CNT/Ni nanospheres.

Before each UV-vis measurement, the catalyst was magnetically separated using external magnate from the reaction mixture before measurement and transferred to 3 mL quartz cuvette.

For comparative analysis, the catalytic performance of Ni nanospheres, carbon-wrapped Ni nanospheres, and CNT/Ni nanospheres was evaluated under identical conditions. Additionally, the presence of 4-NP was independently confirmed by preparing a solution containing 300 μL of a 1 mM 4-NP solution in 6 mL of DI water. This solution was analyzed using UV-vis spectroscopy, with an absorbance peak at 317 nm, without the addition of $NaBH_4$ solution.

The stability and reusability of the carbon-wrapped CNT/Ni nanosphere catalyst were assessed over multiple cycles of the reduction reaction. The catalyst was magnetically separated, rinsed with DI water, and reused in subsequent experiments without drying for reusability studies after every cycle.

3. Results and discussion

3.1 Structural studies by XRD and Raman

The structural characteristics of the synthesized nanomaterials were investigated using X-ray diffraction (XRD) and Raman spectroscopy. Fig. 2(a) displays the XRD patterns of Ni, C-wrapped Ni, CNT/Ni, and C-wrapped CNT/Ni nanospheres. Three prominent diffraction peaks are observed at $2\theta = 44.5°$, 51.8°, and 76.4°, which correspond to the (111), (200), and (220) planes of pure face-centered cubic (fcc) nickel, respectively, as specified by the standard PDF card no. 04-0850. Using the Debye–Scherrer method, the average crystallite size of the Ni nanospheres was estimated to be between 24 nm and 30 nm, based on the most intense (111) diffraction peak.

The presence of CNTs and carbon coating in the synthesized nanomaterials was confirmed by Raman spectroscopy, as shown in Fig. 2(b). In the spectrum of CNT/Ni, two major peaks corresponding to the D and G bands were observed, confirming the presence of CNT. The G band, located around 1531 cm^{-1}, is associated with the E_{2g} vibration mode of the graphitic lattice, while the D band, appearing at approximately 1337 cm^{-1}, corresponds to the A_{1g} vibration mode, indicative of defects or disorder in the sp^2 hybridized carbon structure of CNTs, consistent with previous studies.[34] The Raman spectrum of the C-wrapped CNT/Ni nanospheres exhibits a strong peak at 1769 cm^{-1}, attributed to the stretching vibration of the C=C bond in sp^2 carbon within the carbon wrapping. It also shows distinct CNT-related bands, like those in the CNT/Ni spectrum, suggesting that the carbon coating process did not alter the chemical structure of the CNTs. However, the reduced intensity of these peaks in the C-wrapped CNT/Ni spectrum is likely due to the additional carbon layer on the surface.

3.2 Morphological characterization

The morphological features of the prepared samples were analyzed using Field Emission Scanning Electron Microscopy (FESEM) at various magnifications, as shown in Fig. 3(a–c). The FESEM image of the Ni nanosphere in Fig. 3(a) reveals the formation of predominantly spherical Ni structures with some nanoflake-like formations. The bare Ni nanospheres exhibit an amorphous cluster morphology with scattered pores and spiky surfaces. These surface features could potentially lead to aggregation during the reduction process and contribute to the instability of the nanospheres. The C-wrapped Ni nanosphere in Fig. 3(b) shows a well-dispersed core–shell structure with enhanced surface activity and stability due to the uniform carbon layer. In contrast, Fig. 3(c) illustrates the FESEM image of the C-wrapped CNT/Ni nanosphere, which demonstrates a well-dispersed structure where Ni nanospheres are uniformly integrated with CNTs and enveloped in a consistent carbon coating. This uniform carbon layer and the fine immobilization of Ni nanospheres onto CNTs are expected to facilitate effective electron transport during catalytic reactions. The pre-synthesized Ni nanospheres likely serve as nucleation sites for the formation of the C-wrapped CNT/Ni nanospheres. The CNTs interact with both the Ni nanospheres and the carbon coating, wrapping around them during the hydrothermal treatment,

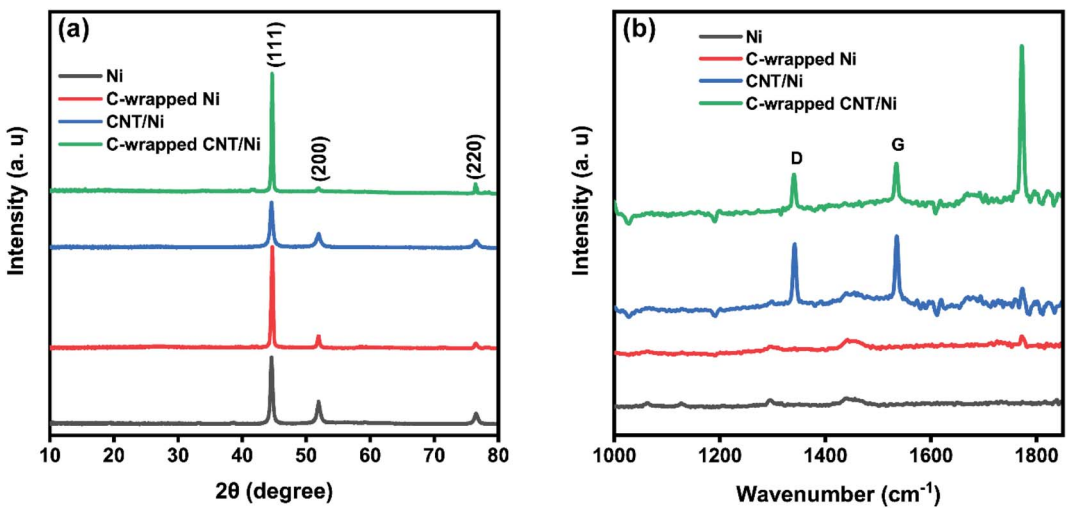

Fig. 2 (a) XRD spectra and (b) Raman spectra of Ni, C-wrapped/Ni, CNT/Ni, and C-wrapped CNT/Ni nanospheres.

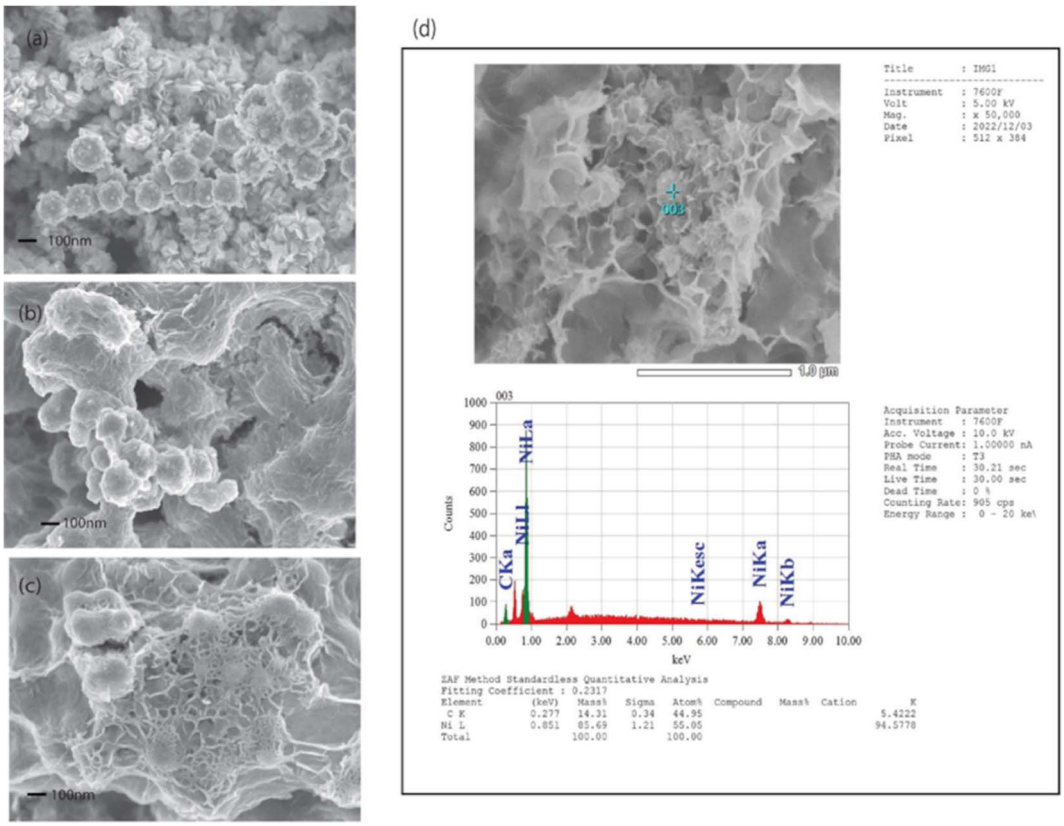

Fig. 3 (a) FESEM images of Ni nanosphere, (b) C-wrapped Ni nanosphere, and (c) C-wrapped CNT/Ni nanosphere, with (d) EDS analysis of C-wrapped CNT/Ni nanosphere.

which promotes carbon growth over the Ni and CNT structures. The resulting synergy between the well-dispersed Ni nanospheres and the interconnected CNT network is anticipated to enhance the catalytic efficiency in the reduction of 4-nitrophenol (4-NP) to 4-aminophenol (4-AP).

3.3 Catalytic reduction of 4-NP to 4-AP

Elemental analysis of the C-wrapped CNT/Ni nanospheres was conducted using energy-dispersive X-ray spectroscopy (EDS), as depicted in Fig. 3(d). The EDS spectrum shows distinct peaks at 0.277 keV and 0.851 keV, corresponding to the K-shell of carbon (C) and the L-shell of nickel (Ni), respectively. The quantitative analysis from the EDS data reveals a carbon content of 44.95% and a nickel content of 55.05%, confirming the successful integration of both elements within the nanospheres.

To assess the catalytic performance of the C-wrapped CNT/Ni nanosphere, we used the reduction of 4-nitrophenol (4-NP) to 4-aminophenol (4-AP) as a model reaction, employing $NaBH_4$ as the hydrogen source. The reaction progress was monitored using UV-visible absorption spectroscopy to track changes in the absorbance characteristics of the substrates and products.

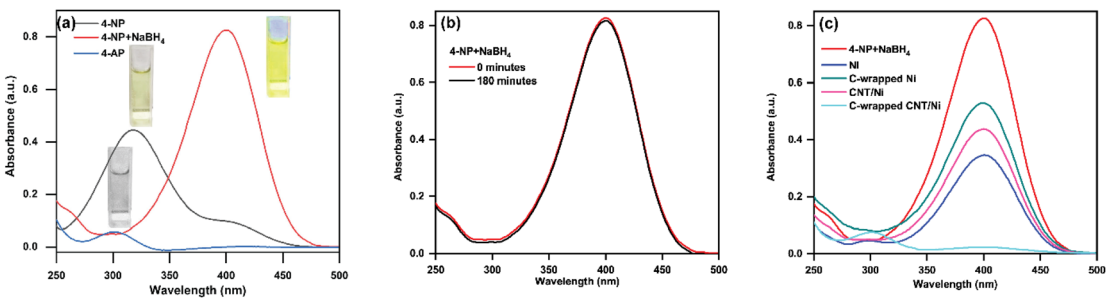

Fig. 4 (a) UV-vis absorption spectra of 4-NP, 4-NP + $NaBH_4$, and 4-AP. (b) UV-vis absorption spectra of 4-NP reduction by $NaBH_4$ without a catalyst. (c) Reduction of 4-NP with Ni, C-wrapped Ni, CNT/Ni, and C-wrapped CNT/Ni as catalysts. The reaction conditions included a temperature of 25 °C, with the pH starting at 10.2 (before catalyst added) and slightly increasing to 10.3 by the end of the reaction (after catalysis).

Initially, the 4-NP solution[2] appeared light yellow with an absorption peak at 317 nm. Upon reduction, the product, 4-AP, showed a peak at 300 nm, as illustrated in Fig. 4(a). The addition of $NaBH_4$ to the solution converts 4-NP into a 4-nitrophenolate ion,[2] leading to a darker yellow color and an absorption peak at 400 nm, as shown in Fig. 4(a). The reduction process was monitored by observing the changes in the 400 nm absorption peak. In the absence of a catalyst, the peak intensity at 400 nm remained unchanged over 3 hours, as depicted in Fig. 4(b). Fig. 4(c) presents the absorption spectra of 4-nitrophenolate ions for different nanocomposites: Ni, C-wrapped Ni, CNT/Ni, and C-wrapped CNT/Ni. The presence of any nanocomposite results in a rapid decrease in the 400 nm peak intensity, with the C-wrapped CNT/Ni showing the most significant reduction rate. This indicates that the catalyst, particularly C-wrapped CNT/Ni nanosphere, is crucial for the effective reduction of 4-NP to 4-AP.

Fig. 5(a) demonstrates the continuous decrease in absorption peak intensity at 400 nm over time with the C-wrapped CNT/Ni nanospheres. Notably, the reaction produced abundant bubbles and a new peak at 300 nm, corresponding to the amine.

The complete disappearance of the 400 nm peak within 20 minutes signifies full reduction of 4-NP. The reaction mixture changed color from bright yellow to colorless, highlighting the superior catalytic activity of the C-wrapped CNT/Ni compared to bare Ni nanospheres. The enhanced catalytic activity is attributed to carbon capping and the interconnected CNT with Ni nanospheres, which provide a larger surface area for hydrogenation and efficient reduction of nitro groups. In contrast, bare Ni nanospheres, although capable of reducing 4-NP to 4-AP, did so at a slower rate. After 90 minutes, the reduction was incomplete (Fig. 5(b)), underscoring the higher catalytic efficiency of the C-wrapped CNT/Ni nanosphere.

The kinetics of the reactions are anticipated to follow pseudo-first-order kinetics due to the significant concentration difference between $NaBH_4$ and the aromatic nitro compounds in the reaction system.[2] Additionally, the concentration of $NaBH_4$ remains relatively constant throughout the reaction. To evaluate the efficiency of the prepared nanocatalysts, pseudo-first-order kinetics are applied. The reaction process is described by the following equation.[2]

$$\ln\frac{C_t}{C_0} = \ln\frac{A_t}{A_0} = -k_{app}t \quad (1)$$

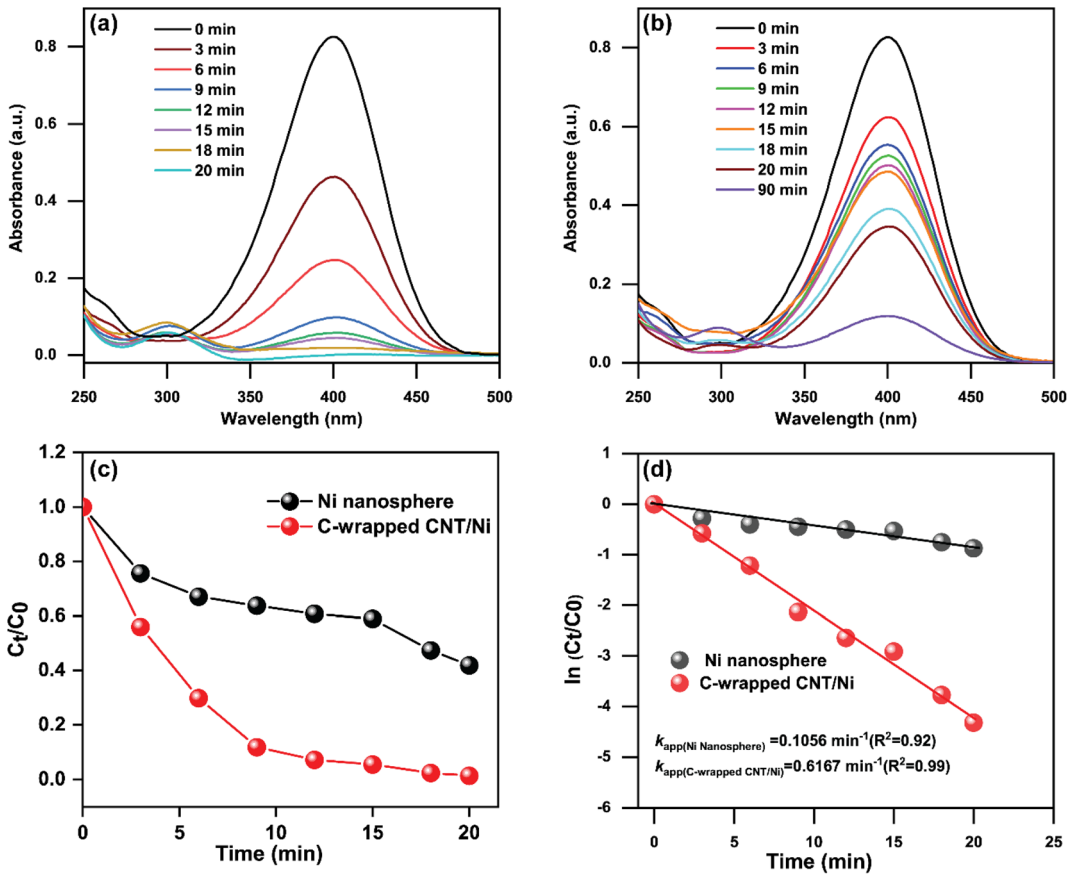

Fig. 5 Time-dependent UV-vis spectral changes during the catalytic reduction of 4-NP to 4-AP using $NaBH_4$ with (a) C-wrapped CNT/Ni nanosphere and (b) Ni nanosphere. Comparative pseudo-first-order kinetic analysis: (c) plot (C_t/C_0) *vs.* reaction time and (d) $\ln(C_t/C_0)$ *vs.* time (s) for the conversion of 4-NP to 4-AP using Ni and C-wrapped CNT/Ni nanosphere. The reaction was conducted at a temperature of 25 °C, with an initial pH of 10.2 and a final pH of 10.3.

Table 1 Summary of the correlation coefficient of $\ln(C_t/C_0)$ *vs.* time plot, rate constant, and activity parameter for the reduction of nitroarenes as-prepared heterogeneous nanocatalyst

Catalyst	Rate constant k (min^{-1})	Activity parameter, K (mg^{-1} min^{-1})	R^2	Conversion (%)
Ni nanosphere	0.1056	0.0264	0.95	58
C-wrapped CNT/Ni nanosphere	0.6167	0.1542	0.99	98

Here, C_t/C_0 is obtained from the relative absorbance intensity A_t/A_0, where A_t and A_0 represent the absorbance values at time t and $t = 0$, respectively. The apparent rate constant, k_{app}, is determined by plotting $\ln(C_t/C_0)$ against time, as shown in Fig. 5(d). This plot exhibits a strong linear correlation, with the slope corresponding to the rate constant. The calculated rate constant k is 0.6167 min^{-1}, which is six times higher than that of bare Ni nanospheres.

The activity parameter K is defined and determined as a normalized rate constant,[2] as given by:

$$K\left(mg^{-1}\ min^{-1}\right) = \frac{k}{m} \quad (2)$$

where k is the rate constant, and m is the amount of the catalyst. The rate constant and activity parameter values for both bare Ni nanospheres and C-wrapped CNT/Ni nanospheres are summarized in Table 1.

In comparison to other reported nanocatalysts, the C-wrapped CNT/Ni nanosphere catalysts fabricated in this study exhibit superior catalytic activity. This is evident from the facile synthesis route and the high-rate constant values obtained for the reduction of 4-nitrophenol (4-NP) to 4-aminophenol (4-AP). For instance, Jiang *et al.* reported that CTAB-modified Ni nanoparticles, with various sizes and morphologies, achieved a rate constant (k) of [j]0.06 min^{-1}, which is lower than that of our prepared nanocatalysts.[11] Similarly, Toyama *et al.* synthesized Ni/SG-SWCNTs using the super-growth method and reported a rate constant of 0.083 min^{-1}, which is seven times lower than that of the C-wrapped CNT/Ni nanosphere.[31] Additionally, Sahoo *et al.* reported a reduced graphene oxide (RGO)/PtNi nanocatalyst[35] with a rate constant of 0.067 min^{-1}. Table 2 provides a comparative summary of catalytic activities between our work and previous reports. The C-wrapped CNT/Ni nanospheres demonstrate significantly higher catalytic activity, as indicated by their values and activity parameters, compared to reported Ni catalysts and many noble metal-based catalysts in the literature. This evidence underscores that the novel and straightforward approach used to fabricate the C-wrapped CNT/Ni nanosphere results in a highly efficient nanocatalyst for the reduction of nitroaromatics.

3.4 Probable catalytic reduction mechanism over C-wrapped CNT/Ni nanospheres

The catalytic reduction of 4-NP using C-wrapped CNT/Ni nanospheres primarily involves hydrogenation occurring on the surface of the Ni nanospheres. Notably, while carbon and CNT do not act as direct catalysts in the reduction process, their roles are crucial. The carbon capping around the Ni nanospheres is essential for immobilizing and well-dispersing the Ni

Table 2 Comparison of the catalytic activities of the nanocatalysts for the reduction of 4-NP

Catalyst	Concentration of 4-NP	Amount of catalyst	Rate constant (k)	Activity parameter (K)	References
RANEY® Ni	0.1 mM	3 mg	[j]0.019 min^{-1} ([i]0.32 × 10^{-3} s^{-1})	[h]N.D.	11
Ni/CTAB	0.1 mM	3 mg	[j]0.06 min^{-1} ([i]1.0 × 10^{-3} s^{-1})	[h]N.D.	
Ni/SG-SWCNTs[a]	2.0 mM	15 mg	0.083 min^{-1}	0.0055 mg^{-1} min^{-1}	31
Ni/MC[b]-750	0.01 M	0.3 mg	[j]0.376 min^{-1} ([i]6.26 × 10^{-3} s^{-1})	[j]1.254 mg^{-1} min^{-1} ([i]20.9 g^{-1} s^{-1})	36
Ni/rGO[c]	0.5 mM	2.0 mg	[j]0.459 min^{-1} ([i]7.66 × 10^{-3} s^{-1})	[h]N.D.	37
Ni/NCMTs[d]-500	0.1 mM	1 mg	[j]0.342 min^{-1} ([i]5.7 × 10^{-3} s^{-1})	[j]8.34 mg^{-1} min^{-1} ([i]139 × 10^{-3} mg^{-1} s^{-1})	38
Ni/NCMTs[d]-800	0.1 mM	1 mg	[j]0.522 min^{-1} ([i]8.7 × 10^{-3} s^{-1})	[j]4.26 mg^{-1} min^{-1} ([i]71 × 10^{-3} mg^{-1} s^{-1})	
Ni/NCMTs[d]-900	0.1 mM	1 mg	[j]0.252 min^{-1} ([i]4.2 × 10^{-3} s^{-1})	[j]1.92 mg^{-1} min^{-1} ([i]32 × 10^{-3} mg^{-1} s^{-1})	
Ni/rGO[c]@Au	5.0 mM	3 mg	[j]0.524 min^{-1} ([i]8.73 × 10^{-3} s^{-1})	[j]0.582 mg^{-1} min^{-1} ([i]9.7 g^{-1} s^{-1})	39
DE[e]/Ni/N-C[f]-800	5.0 mM	3 mg	[j]2.1 min^{-1} ([i]35 × 10^{-3} s^{-1})	[j]3.18 mg^{-1} min^{-1} ([i]0.053 mg^{-1} s^{-1})	40
RGO[c]/PtNi	5.0 mM	3 mg	0.067 min^{-1} ([j]1.12 × 10^{-3} s^{-1})	[h]N.D.	35
g-C_3N_4[g]@Ni$_3$C_600	5.0 mM	23 mg	0.383 min^{-1} ([j]6.383 × 10^{-3} s^{-1})	[h]N.D.	17
C-wrapped CNT/Ni nanosphere	**1.0 mM**	**4 mg**	**0.6167 min^{-1} ([j]10.283 × 10^{-3} s^{-1})**	**0.1542 $mg^{-1}min^{-1}$ ([j]2.57 $g^{-1}s^{-1}$)**	**This work**

[a] Super-growth single wall carbon nanotube. [b] Mesoporous carbon. [c] Reduced graphene oxide. [d] N-doped carbon microtubes. [e] Diatomite. [f] Nitrogen-doped carbon. [g] Graphite-like carbon nitride. [h] Not defined. [i] Standardized/converted from original given data in article. [j] Obtained/reported from original data given in article.

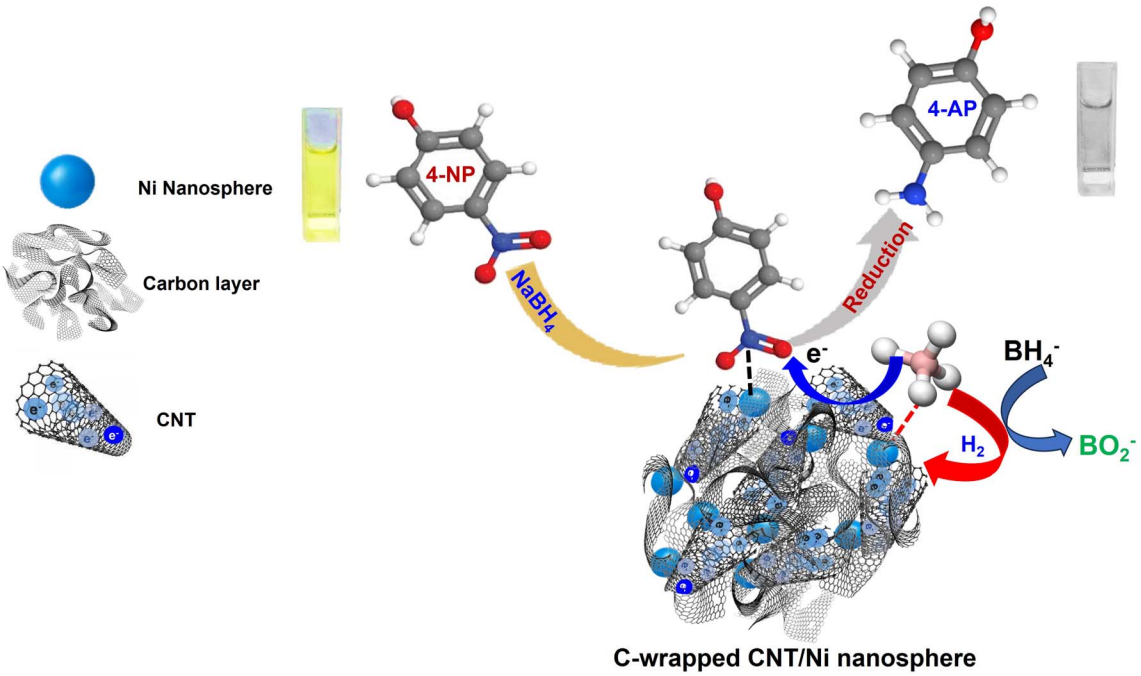

Fig. 6 Proposed mechanism for the catalytic reduction of 4-NP by $NaBH_4$ on the C-wrapped CNT/Ni nanosphere catalyst in an aqueous medium.

particles, which provides a large surface area with numerous activated sites for efficient absorption and desorption of reactants and products. Additionally, the interconnected CNTs between the Ni nanospheres and the carbon layer contribute to a robust structure and create a favourable environment for the hydrogenation reduction reaction through synergistic effects. This setup may also affect the standard reduction potential of Ni and establish shorter pathways for H^+ reduction.

The proposed mechanism for the catalytic reduction of 4-NP by the C-wrapped CNT/Ni nanospheres is illustrated in Fig. 6. The process involves the following steps: (i) *reaction initiation*: borohydride ions (BH_4^-) react with water to produce borate ions (BO_2^-) and hydrogen gas. The hydrogen adsorbed on the surface of the C-wrapped CNT/Ni nanospheres facilitates the formation of a hydride complex with Ni, making it an active reductant. (ii) *Adsorption and reduction*: the 4-nitrophenolate anions adsorb onto the carbon layer and CNT, positioning the substrate close to the active Ni reductant. Atomic exchange and electron transfer between BH_4^- and 4-NP occur, resulting in the formation of 4-AP. During this process, the active reductant is oxidized, and electrons are rapidly transferred through the CNT and carbon layer to the 4-nitrophenolate anions, accelerating the reduction of 4-NP to 4-AP, and (iii) *catalyst regeneration*: after the reduction, the product detaches from the Ni nanosphere surface, exposing new active sites for further reactions. The Ni nanospheres are critical in this reaction as they provide multiple sites for adsorption and help lower the kinetic energy barrier of the reduction. Overall, the C-wrapped CNT/Ni nanospheres exhibit excellent catalytic performance for the conversion of 4-NP to 4-AP, demonstrating their effectiveness in facilitating this reaction.

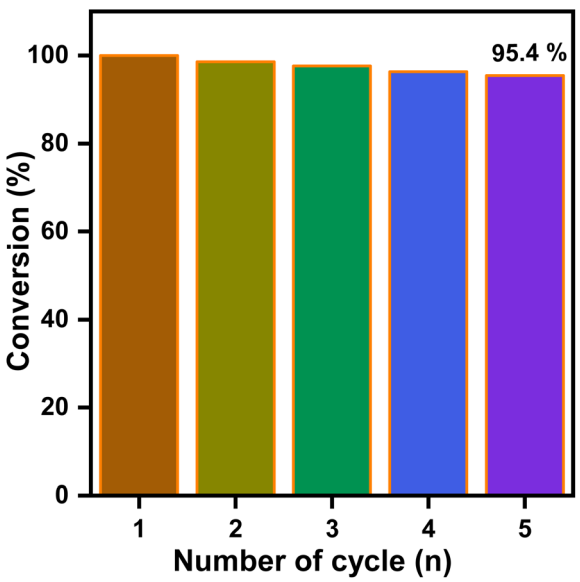

Fig. 7 The reusability of the C-wrapped CNT/Ni nanosphere for the reduction of 4-NP in the presence of $NaBH_4$ solution. The reaction was performed under controlled conditions at a temperature of 25 °C, with an initial pH of 10.2, which increased slightly to pH of 10.3.

3.5 Reusability of the C-wrapped CNT/Ni nanosphere catalyst

To evaluate the reusability of the C-wrapped CNT/Ni nanosphere catalyst, we selected the reduction of 4-nitrophenol (4-NP) as the model reaction. After each reaction cycle, the catalyst was separated from the reaction mixture and reused for five

consecutive cycles. The results, as depicted in Fig. 7, show only a minimal decline in catalytic activity.

After five cycles, the catalytic efficiency of the C-wrapped CNT/Ni nanosphere decreased slightly to 95.4%. This high stability can be attributed to the effective dispersion of Ni nanospheres within the carbon nanosheets, which provides a large surface area with numerous activated sites and facilitates the desorption of 4-aminophenol (4-AP) from the catalyst surface. Additionally, the interconnected CNTs and the carbon layer contribute to a robust structure and an optimal environment for the hydrogenation reduction reaction. The strong magnetic properties of the materials also enable easy recycling and separation, significantly enhancing their reusability across multiple cycles.

4. Conclusions

The successful synthesis of magnetically retrievable C-wrapped CNT/Ni nanospheres was achieved using a novel and straightforward method. The resulting nanospheres exhibited well-defined crystallinity and controlled aggregation, resulting in a uniform distribution of Ni nanospheres within the carbon-wrapped CNT structure. The synergistic effects of the nanospherical Ni, the carbon coating, and the interconnected CNTs contribute to the excellent catalytic performance of the C-wrapped CNT/Ni nanospheres for the reduction of 4-nitrophenol (4-NP). Notably, these nanospheres demonstrate high recyclability, underscoring their potential for environmental remediation applications. The simplicity, controllability, and cost-effectiveness of this synthetic technique, which integrates wrapped carbon, CNTs, and nanospherical Ni, highlights its promise for practical use.

Data availability

The information utilized to support the findings of this research may be found within the paper. The associated author is willing to provide more information upon reasonable request that supports the results of these findings.

Conflicts of interest

There are no conflicts of interest to declare.

Acknowledgements

This research is funded by the Centre for Advanced Scientific Research (CASR) of Bangladesh University of Engineering and Technology (BUET), Dhaka, Bangladesh. The authors also acknowledge partial support from grants for Advanced Research in Education, Ministry of Education, Government of Bangladesh.

References

1 H. Zhao, T. Ouyang, Y. Li, W. Dong, Q. Duan and T. Fei, *ACS Appl. Nano Mater.*, 2023, **6**, 22989–22997.
2 Y. Kumar, S. Rani, J. Shabir and L. S. Kumar, *ACS Omega*, 2020, **5**, 13250–13258.
3 N. Anusuya, C. Pragathiswaran and G. Thulasi, *Mater. Today: Proc.*, 2021, **37**, 3759–3763.
4 P. Fan, X. Zhang, H. Deng and X. Guan, *Appl. Catal., B*, 2021, **285**, 119829.
5 L. Song, L. Shu, Y. Wang, X. F. Zhang, Z. Wang, Y. Feng and J. Yao, *Int. J. Biol. Macromol.*, 2020, **143**, 922–927.
6 A. Ghosh, M. Khurana, A. Chauhan, M. Takeo, A. K. Chakraborti and R. K. Jain, *Environ. Sci. Technol.*, 2010, **44**, 1069–1077.
7 N. Modirshahla, M. A. Behnajady and S. Mohammadi-Aghdam, *J. Hazard. Mater.*, 2008, **154**, 778–786.
8 F. T. Bekena, H. Abdullah, D.-H. Kuo and M. A. Zeleke, *J. Ind. Eng. Chem.*, 2019, **78**, 116–124.
9 G. Fadillah, T. A. Saleh and S. Wahyuningsih, *J. Mol. Liq.*, 2019, 289.
10 H. Hu, J. H. Xin, H. Hu, X. Wang, D. Miao and Y. Liu, *J. Mater. Chem. A*, 2015, **3**, 11157–11182.
11 Z. Jiang, J. Xie, D. Jiang, X. Wei and M. Chen, *CrystEngComm*, 2013, **15**, 560–569.
12 G.-M. Shi, S.-T. Li, F.-N. Shi, X.-F. Shi, S.-H. Lv and X.-B. Cheng, *Colloids Surf., A*, 2018, **555**, 170–179.
13 K. Zhang, J. M. Suh, J. W. Choi, H. W. Jang, M. Shokouhimehr and R. S. Varma, *ACS Omega*, 2019, **4**, 483–495.
14 X. Lin, M. Wu, S. Kuga, T. Endo and Y. Huang, *Polym. J.*, 2016, **48**, 919–923.
15 Z. Hasan, Y. S. Ok, J. Rinklebe, Y. F. Tsang, D.-W. Cho and H. Song, *J. Alloys Compd.*, 2017, **703**, 118–124.
16 T. Guo, C. Wang, N. Zhang, Y. Zhang, T. Chen, X. Xing, Z. Lu and L. Wen, *Cryst. Growth Des.*, 2020, **20**, 6217–6225.
17 M. Liu, B. Niu, H. Guo, S. Ying and Z. Chen, *Inorg. Chem. Commun.*, 2021, **130**, 108687.
18 R. Prasad, M. K. Lolakshi and B. R. Bhat, *Synth. Met.*, 2016, **219**, 26–32.
19 L. Liu, R. Chen, W. Liu, J. Wu and D. Gao, *J. Hazard. Mater.*, 2016, **320**, 96–104.
20 Z. Xu, X. He, M. Liang, L. Sun, D. Li, K. Xie and L. Liao, *Mater. Chem. Phys.*, 2019, **227**, 64–71.
21 L. Xiong, Y. Fu, Y. Luo, Y. Wei, Z. Zhang, C. Wu, S. Luo, G. Wang, D. Sawtell, K. Xie, T. Wu, D. Ding and L. Huang, *J. Mater. Res.*, 2022, **37**, 2109–2123.
22 V. Polshettiwar, R. Luque, A. Fihri, H. Zhu, M. Bouhrara and J.-M. Basset, *Chem. Rev.*, 2011, **111**, 3036–3075.
23 Y. Zhai, Y. Dou, X. Liu, S. S. Park, C.-S. Ha and D. Zhao, *Carbon*, 2011, **49**, 545–555.
24 M. R. Islam, M. Ferdous, M. I. Sujan, X. Mao, H. Zeng and M. S. Azam, *J. Colloid Interface Sci.*, 2020, **562**, 52–62.
25 Y. Zhao, B. Cao, X. Wang, X. Wang, M. Al-Mamun, H. Zhao, J. Wang, Y. Zheng and X. Su, *J. Environ. Chem. Eng.*, 2018, **6**, 5239–5248.
26 M. J. Ndolomingo, N. Bingwa and R. Meijboom, *J. Mater. Sci.*, 2020, **55**, 6195–6241.
27 Y. Wang, Z. Rong, Y. Wang, P. Zhang, Y. Wang and J. Qu, *J. Catal.*, 2015, **329**, 95–106.

28 J. Xiao, X. Pan, F. Zhang, H. Li and X. Bao, *Chem. Sci.*, 2017, **8**, 278–283.
29 Z. Guan, S. Lu and C. Li, *J. Catal.*, 2014, **311**, 1–5.
30 H. Veisi, S. Kazemi, P. Mohammadi, P. Safarimehr and S. Hemmati, *Polyhedron*, 2019, **157**, 232–240.
31 N. Toyama, H. Kimura, N. Matsumoto, S. Kamei, D. N. Futaba, N. Terui and S. Furukawa, *Nanotechnol.*, 2021, **33**, 065707.
32 Y. Qu, G. Xu, J. Yang and Z. Zhang, *Appl. Catal., A*, 2020, **590**, 117311.
33 J. Y. Choi, Y. K. Lee, S. M. Yoon, H. C. Lee, B. K. Kim, J. M. Kim, K. M. Kim and J. H. Lee, *J. Am. Ceram. Soc.*, 2005, **88**, 3020–3023.
34 J.-M. Feng and Y.-J. Dai, *Nanoscale*, 2013, **5**, 4422–4426.
35 P. K. Sahoo, B. Panigrahy and D. Bahadur, *RSC Adv.*, 2014, **4**, 48563–48571.
36 Y. Yang, Y. Ren, C. Sun and S. Hao, *Green Chem.*, 2014, **16**, 2273–2280.
37 Y. Li, Y. Cao and D. Jia, *J. Nanopart. Res.*, 2018, **20**, 1–8.
38 J. Wang, M. Zhang, T. Miao, Y. Ling, Q. Wen, J. Zheng, J. Xu, T. Hayat and N. S. Alharbi, *Inorg. Chem. Front.*, 2018, **5**, 844–852.
39 M. Cao, L. Feng, P. Yang, H. Wang, X. Liang and X. Chen, *J. Mater. Sci.*, 2017, **53**, 4874–4883.
40 D. B. Jiang, X. Liu, Y. Yuan, L. Feng, J. Ji, J. Wang, D. Losic, H.-C. Yao and Y. X. Zhang, *Chem. Eng. J.*, 2020, **383**, 123156.